RESEARCH ARTICLE | NOVEMBER 12 2024

Link between permanent shear-banding and local concentration fluctuations in suspensions of compressible microgels

Gavino Bassu ; Judith E. Houston ; Mayra A. Lara-Peña ; Hartmut Kriegs ; Minne Paul Lettinga ; Lionel Porcar ; Andrea Scotti ; Marco Laurati

Physics of Fluids 36, 113116 (2024)
https://doi.org/10.1063/5.0237526

Physics of Fluids ARTICLE pubs.aip.org/aip/pof

Link between permanent shear-banding and local concentration fluctuations in suspensions of compressible microgels

Cite as: Phys. Fluids **36**, 113116 (2024); doi: 10.1063/5.0237526
Submitted: 5 September 2024 · Accepted: 21 October 2024 ·
Published Online: 12 November 2024

Gavino Bassu,[1,2] Judith E. Houston,[3] Mayra A. Lara-Peña,[4] Hartmut Kriegs,[5] Minne Paul Lettinga,[5,6] Lionel Porcar,[7] Andrea Scotti,[8,a)] and Marco Laurati[1,2,a)]

AFFILIATIONS

[1]Dipartimento di Chimica "Ugo Schiff", Università di Firenze, via della Lastruccia 3, Sesto Fiorentino (FI) 50019, Italy
[2]Consorzio per lo Sviluppo dei Sistemi a Grande Interfase (CSGI), via della Lastruccia 3, Sesto Fiorentino (FI) 50019, Italy
[3]European Spallation Source ERIC, Box 176, SE-22100 Lund, Sweden
[4]División de Ciencias e Ingenierías, Universidad de Guanajuato, Lomas del Bosque 103, 37150 León, Mexico
[5]Biological Information Processing IBI-4, Forschungszentrum Jülich, Jülich 52425, Germany
[6]Laboratory for Soft Matter and Biophysics, KU Leuven, B-3001 Leuven, Belgium
[7]Institut Laue-Langevin ILL, DS/LSS, 71 Avenue des Martyrs, F-38000 Grenoble, France
[8]Division of Physical Chemistry, Lund University, SE-22100 Lund, Sweden

[a)]**Authors to whom correspondence should be addressed:** andrea.scotti@fkem1.lu.se and marco.laurati@unifi.it

ABSTRACT

We uncover the occurrence of shear banding in dense suspensions of compressible microgels. Velocimetry measurements evidence the presence of permanent but unsteady shear-banding for sufficiently small Peclet numbers, with the formation of a central plug-like flow. Small-angle neutron scattering experiments under shear link the observed banding phenomenon to structural variations along the velocity gradient, providing a connection between the arrested band and the increase in structural correlations associated with changes in the local packing fraction. This provides unique evidence of a shear–concentration coupling mechanism in jammed suspensions of compressible particles.

I. INTRODUCTION

Shear banding, i.e., the formation of bands with different local values of the shear rate $\dot{\gamma}$, is a phenomenon that has been reported for a variety of complex fluids, including polymer solutions and melts, emulsions, foams, colloidal, and granular suspensions.[1,2] Soft glassy materials (SGMs)[3] are amorphous solids formed by dense assemblies of colloidal particles. SGMs flow under shear when a stress larger than a threshold value, called yield stress,[4] is applied to them. Shear banding in SGMs can be a transient phenomenon followed by homogeneous flow[5–7] that could originate from structural differences between the transient band and the rest of the sample.[8]

Band formation under flow is also observed in steady state, but a clear understanding of the physical laws that govern this phenomenon is still elusive. Mechanisms invoked to explain the band formation are (i) competition between shear rejuvenation and aging induced by aggregation or thermally activated processes,[9–11] (ii) the coexistence between a static and dynamic yield stress,[12,13] and (iii) a coupling between fluctuations in the local concentration and $\dot{\gamma}$, in which spatial variations of the local shear rate induce a mass flux and thus a change in the local concentration and local yield stress value, resulting in shear localization through a feedback mechanism.[14,15] Local variations of the concentration have been also linked to vorticity banding observed in surfactant solutions forming lamellar phases.[16] Although the latter mechanism has often been used to explain shear-banding in glasses of incompressible colloids,[15,17,18] its experimental observation remains challenging due to the subtle variations in local packing fraction involved for hard sphere-like suspensions. The compressibility of an individual colloid, like a microgel,[19] could enhance these fluctuations,

allowing them to be observed experimentally. Dense microgel suspensions constitute an important class of SGMs in which the rheological properties are linked to the particle softness and its evolution as a function of packing.[20–22] While the presence of transient shear banding in microgel suspensions has been demonstrated for carbopol microgels,[5] and interpreted in terms of fluidity models of simple yield stress fluids,[23] steady-state banding remained elusive. Only partial, unconfirmed indications have been presented for transient shear banding in poly-*N*-isopropylacrylamide (PNIPAM) microgel suspensions.[24]

Here, we report experimental velocimetry measurements for overcrowded suspensions of PNIPAM-based microgels that evidence the presence of permanent but unsteady shear banding, observed at sufficiently low shear rates and characterized by profile fluctuations. The structural variations along the velocity gradient are directly measured by combining shear and small-angle neutron scattering (SANS) in the flow direction using a custom-designed flow cell.[25] Our data show that band formation is associated with changes in the local packing fraction, i.e., to shear–concentration coupling. In this concentration regime interpenetration,[26] deswelling[27] and deformation[28] lead to microgel hardening,[20,22] indicating that the degree of particle softness plays an important role in both the band formation and in the extent of the structural variations. The sample consists of a microgel suspension with an effective volume fraction $\phi_{\text{eff}} \approx 1.3$, deep in the jammed state.[29,30] Additional details on the microgels and suspension preparation can be found in Sec. II. All measurements were performed at a constant temperature T = 20 °C.

II. METHODS

A. Sample preparation

Microgels composed of poly(*N*-isopropylacrylamide) (PNIPAM) and poly(ethylene glycol) methyl ether methacrylate (PEGMA) in a weight fraction equal to 30% PEGMA and 70% PNIPAM were synthesized as in Refs. 29–31 using ethylene glycol dimethacrylate (EGDMA) as crosslinker (1% mole fraction). The microgels were dispersed in H_2O (velocimetry experiments) or D_2O (Rheo-SANS experiments) at a concentration c = 18.6 ± 0.1% w/w. Particles have an average radius equal to 140±10 nm and a size polydispersity of 25±2%, as determined from SANS measurements of a dilute suspension.[32] Figure S1 in the supplementary material shows that between 20 °C and 25 °C, within errors, the size of the particles is the same in H_2O and D_2O.

B. Rheology

The measurements were performed on a DHR3 stress-controlled rheometer (TA Instruments) using a smooth cone-plate geometry (cone diameter 40 mm, cone angle 2°) for the dynamic frequency sweep, and a 20-mm diameter smooth plate–plate geometry (500 μm gap) for the flow curve and stress growth experiments at different applied shear rates. A shear rate gradient such as that present in the plate–plate geometry is a necessary condition for investigating the shear–concentration coupling mechanism. At the same time, one should take into account that it might have an interplay with the intrinsic banding behavior of the sample. To avoid evaporation, a solvent trap that isolates the sample from the surroundings was used. It consists of an enclosure with a solvent seal at the top and a permanent seal at the bottom, which creates a saturated atmosphere. A rejuvenation protocol was implemented before each measurement to minimize the effects of sample loading and aging. It consists of the following steps: first, oscillatory shear in the form of a dynamic time sweep with a large strain amplitude ($\gamma_0 = 700\%$) was applied for 180 s. The sample showed a liquid-like behavior at the end of this test. Subsequently, the sample was subjected again to oscillatory shear in the form of a dynamic time sweep with a low strain amplitude ($\gamma_0 = 0.05\%$) until a steady state in the viscoelastic moduli was reached. We found that 180 s were sufficient to reach the steady state. In both tests, the frequency used was $\omega = 10$ rad/s. No clear indications of wall slip were observed, as tested from the dependence of the rheological response on the gap used for the plate-plate geometry.

C. Heterodyne DLS measurements of velocity profiles

Heterodyne dynamic light scattering measurements of velocity profiles were performed with a custom made shear cell with a glass concentric cylinder geometry, with the inner and outer cylinders having diameters of 43 and 45 mm, respectively, and the gap being equal to 1 mm. The internal cylinder is rotated to induce flow. The measurements were performed at one central position along the axis of the cell. Temperature of the cell was controlled through immersion in a thermostatic bath containing an optical matching fluid, providing an accuracy of 0.1 °C. Additional details on the heterodyne light scattering setup can be found in Ref. 33. Velocity profiles made of 30 points spanning the 1 mm gap from the rotor to the stator where obtained by performing for each point, i.e., at each position across the gap, a light scattering measurement of duration equal to 10 s to obtain a correlation function. A whole velocity profile spanning the entire gap was obtained in ≈5 min.

D. SANS measurements under shear using the 1,2-shear cell

SANS experiments in the flow-gradient plane were performed using the 1,2-shear cell on the D22 SANS beamline of ILL. Experiments at different shear rates, and at T = 20 °C, were performed in a short gap Couette cell with a 5-mm path length, with moving inner cylinder of radius R1 = 25.0 mm and stationary outer cylinder of radius R2 = 26.0 mm as previously described.[25] No stress measurement can be performed with this shear-cell. Temperature was controlled through a thermostated bath. The flow-SANS experiments were performed at a detector and collimation distance of 17.6 m, with an 8.0-m rectangular collimation (40 × 55 mm^2), $\lambda = 6$ Å neutron wavelength, and a wavelength spread of $\Delta\lambda/\lambda = 10\%$. To spatially resolve different positions along the gap, a stepper motor was used to translate the cell perpendicular to the neutron beam path defined with a 0.1-mm wide curved slit × 3-mm height across the 1.0 mm gap (z_g). Five gap positions ($z/z_g = 0.00$, 0.25, 0.5, 0.75, 1.00) were measured. Measurements at each position were run for a minimum of 45 min (60 min in some cases). All experiments covered a Q-range of 0.0022–0.028 Å^{-1}. Sample transmission measurements were taken at each gap position. The sample was allowed to equilibrate after loading. Measurements at the slowest shear rate were repeated to ensure reproducibility. Data were analyzed and reduced using the ILL GRASP software.

E. Model of the scattering intensity in the quiescent state

The scattering intensity I(q) was modeled using the following expression:

$$I(Q) = \phi V_p \Delta\rho^2 P(Q) S(Q), \quad (1)$$

where ϕ is the microgel packing fraction, V_p is the microgel volume, $\Delta\rho^2$ is the contrast, and $P(Q)$ is the particle form factor that was modeled using a fuzzy sphere term

$$P(Q) = \left[3 \frac{\sin QR_c - QR_c \cos QR_c}{(QR_c)^3} \times \exp\left(-\frac{(\sigma Q)^2}{2} \right) \right], \quad (2)$$

in which R_c is the particle core radius and σ is the fuzziness parameter. Polydispersity in the core radius was included using a Gaussian distribution function with a width σ_p determined from the fit. $S(Q)$ is the interparticle structure factor that was modeled through a Percus–Yevick hard sphere structure factor term. B is a background term.

III. RESULTS AND DISCUSSION

Rheological measurements were used to characterize the bulk response of the suspension. Frequency sweeps measured in the linear viscoelastic regime indicate a solid-like behavior of the suspension [Fig. 1(a), inset]. The flow curve is typical of a yield stress fluid and can be described with the Herschel–Bulkley model,[29] $\sigma = \sigma_y + k(\dot{\gamma})^\nu$ [Fig. 1(a)]. The yield stress and exponent obtained from the fitting are $\sigma_y = 2.6$ Pa, $\nu = 0.52$, with the latter characteristic of dense microgel suspensions.[34] Figure 1(b) shows the results of stress growth experiments at different applied shear rates. For $\dot{\gamma} \leq 0.5\ s^{-1}$, after the initial regime corresponding to linear response and yielding, the stress and viscosity slowly increase with time, indicating that uniform, steady-state flow is not attained. Interestingly, some sudden small jumps in the stress are observed at specific times (Fig. 1 inset, for $\dot{\gamma} = 0.1\ s^{-1}$). The growth becomes less and less pronounced with increasing $\dot{\gamma}$ until disappearing for $\dot{\gamma} = 5\ s^{-1}$, for which uniform flow at constant stress is recovered.

Velocimetry measurements were performed using the heterodyne dynamic light scattering setup described in Ref. 33, equipped with a concentric cylinder geometry. Additional details on the cell setup and measurements can be found in Sec. II. Before starting the measurements, the sample was pre-sheared at a rate of $1\ s^{-1}$ for 300 s. The sample was then left at rest for 600 s to reform a reproducible initial state.[35,36] Velocity profiles were measured at different waiting times t_w after application of the desired shear rate to the sample. The velocity profiles for different shear rates, averaged over measurements performed every 900 s between $t_w = 0$ and 2700 s (the acquisition time of

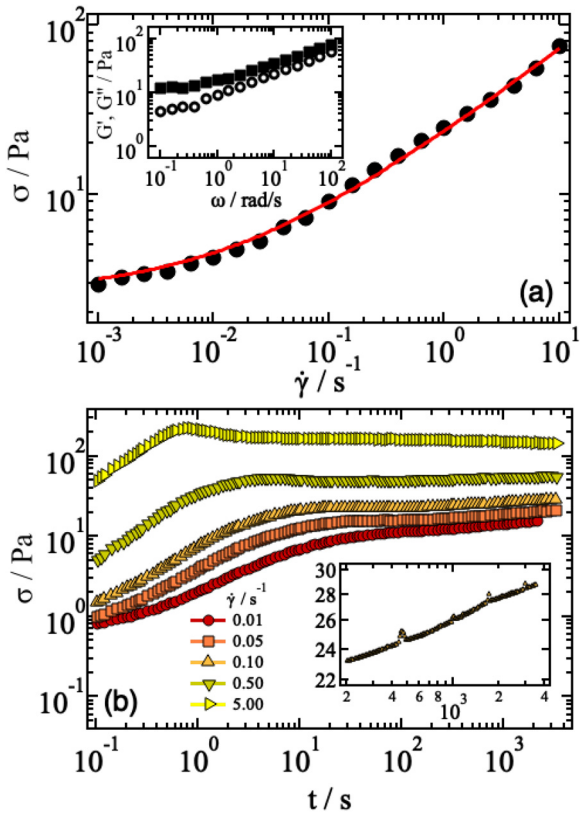

FIG. 1. (a) Flow curve (circles) and fit of a Herschel–Bulkley function (red line). Inset: G' (squares) and G'' (circles) as a function of the frequency ω measured in a dynamic frequency sweep. (b) Stress σ as a function of time t measured in stress growth experiments for different rates, as indicated. Inset: Zoom in the region of long times for $\dot{\gamma} = 0.1\ s^{-1}$, evidencing the presence of sudden small jumps in the stress. All measurements performed at T = 20 °C.

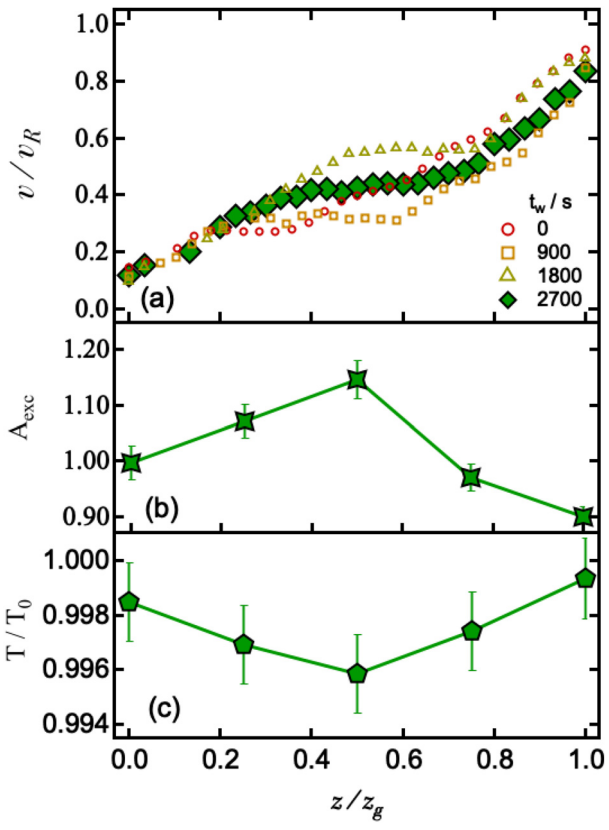

FIG. 2. (a) Normalized velocity profile measured for $\dot{\gamma} = 0.1\ s^{-1}$ ($Pe_0 = 1.1 \times 10^{-3}$), and averaged from $t_w = 0$ s to $t_w = 2.7 \times 10^3$ s (diamonds). Smaller empty symbols correspond to velocity profiles measured for intermediate times (as indicated). (b) Integral of the excess scattering of the sheared sample, as a function of position along the gap and (c) ratio between the transmissions of the sheared (T) and quiescent (T_0) sample measured by SANS.

the Rheo-SANS experiments), show the onset of shear banding when $\dot{\gamma} \leq 0.2\ s^{-1}$. Figure 2(a) reports the representative profiles measured for $\dot{\gamma} = 0.1\ s^{-1}$, data for additional shear rates can be found in Fig. 3. Velocities (v) were normalized to the velocity of the moving rotor (v_R) and the position along the gap z to the gap size z_g. For $\dot{\gamma} = 0.1\ s^{-1}$, the corresponding Peclet number is $Pe_0 = \dot{\gamma}\tau_B = 6\pi\dot{\gamma}\eta R^3/k_BT = 1.1 \times 10^{-3}$, with τ_B the Brownian diffusion time in dilute conditions, $R \approx 140$ nm the particle radius, and η the water viscosity at $T = 20\,^{\circ}C$. Shear banding was observed and predicted for hard-sphere glasses for similar values of Pe_0.[15,17] Shear localization due to strong shear rate gradients[37] can be excluded since the variations of the shear rate and stress due to the size of the gap in Couette geometry are moderate for our shear cell ($R_i/R_o \approx 0.955$, with R_i and R_o being the inner and outer radius, respectively).

The diamonds in Fig. 2(a) correspond to a profile that shows a band presenting plug-like flow for $0.4 \lesssim z/z_g \lesssim 0.6$ instead of close to the static surface at $z/z_g = 0$. The presence of a slight wall slip is also evident from the values of the normalized velocity at the boundaries, which are larger than 0 at the static rotor ($z/z_g \simeq 0$) and smaller than 1 at the moving rotor ($z/z_g \simeq 1$). The simultaneous presence of wall slip and banding has been often reported for SGMs.[1] The presence of shear-banding in the velocity profiles is observed almost immediately after shear startup; however, the shape of the velocity profiles varies significantly over time, showing either stronger localization in the central region [Fig. 2(a), small squares] or approach to a linear profile [Fig. 2(a), small circles]. The formation of the unsheared band in the central region of the gap further supports the absence of shear localization due to strong shear rate gradients. Figure S2 of the supplementary material shows in addition that shear banding persists over times an order of magnitude larger than the $t_w = 2700$ s. The observed shear-banding phenomenon is, therefore, long-lived, but unsteady. Furthermore, at sufficiently large rates ($\dot{\gamma} = 5\ s^{-1}$) and stresses, a linear profile is recovered (Fig. 3) and, as already mentioned, the rheological response evidences homogeneous flow at constant stress [Fig. 1(b)]. Therefore, there is an upper threshold in the rate or stress for observing this shear-banding phenomenon. Similar profiles and shape fluctuations have been previously reported for hard sphere colloidal glasses[17] and interpreted in terms of flow-induced particle migration, without providing, however, experimental evidence for this mechanism.

To investigate the link between the observed shear-banding and structural changes in the microgel suspension, Rheo-SANS experiments were performed on D22 instrument at the Institute Laue-Langevin using their concentric cylinder 1,2-shear cell.[25] Additional details on the shear cell and measurements can be found in the supplementary material. The same rejuvenation protocol used for velocimetry measurements was applied in this case. This setup allowed us to measure scattered intensity profiles at five different points along the velocity gradient, i.e., in the flow direction [Fig. 4(a), sketch]. This is the required scattering plane to detect changes in the intensity I(Q) related to shear-induced restructuring[38] or variations in the velocity gradient associated with shear banding.[39,40] The I(Q)s were measured over 2700 s to accumulate enough statistics for each position and $\dot{\gamma}$.

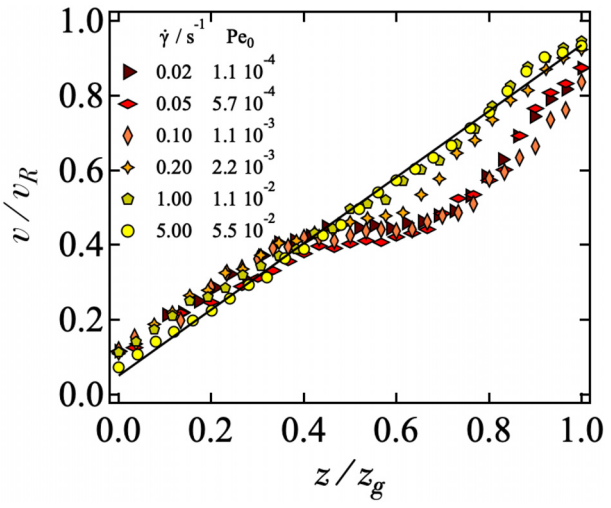

FIG. 3. Velocity profiles measured for different $\dot{\gamma}$ (Pe_0), as indicated, and averaged from $t_w = 0$ s to $t_w = 2.7 \times 10^3$ s. For the largest rate $\dot{\gamma} = 5.0\ s^{-1}$ a linear profile is recovered, as indicated by the solid black line.

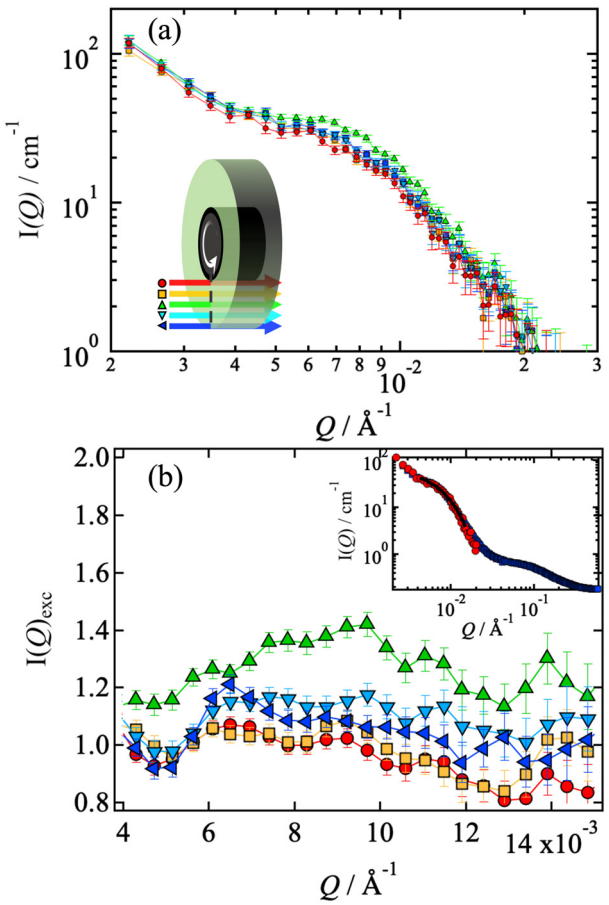

FIG. 4. (a) Scattering intensities I(Q) vs Q measured for a shear rate $\dot{\gamma} = 0.01\ s^{-1}$ and for different positions along the velocity profile, as indicated in the sketch. (b) Corresponding excess scattering intensities vs Q. Inset: Scattering intensity I(Q) vs Q in the quiescent state, measured in the shear cell (red circles) and in a normal cuvette (blue squares). Black line: Fit used to extract the excess scattering intensities (see Sec. II for details).

Data averaged over shorter intervals of 900 s (Fig. S7 of the supplementary material) show similar behavior with larger noise (see supplementary material for more details). The Q-range accessible in this configuration is 2.2×10^{-3} Å$^{-1} \leq Q \leq 2.8 \times 10^{-2}$ Å^{-1}. The I(Q) at rest was measured in a standard cuvette on a broader Q-range. In the common Q-range, these data and those measured with the shear-cell in quiescent conditions nicely overlap [circles and squares in Fig. 4(b), inset].

For the large packing fraction investigated, $\phi_{\text{eff}} \approx 1.3$, the I(Q) of the sample at rest shows the presence of a structure factor [S(Q)] peak around $Q \approx 8 \times 10^{-3}$ Å^{-1}, although the peak is not very pronounced. Indeed, the combination of a soft, Hertzian-like inter-particle potential and polydispersity leads to a decrease in the structural peak in the S(Q) for $\phi_{\text{eff}} \gg 1$.[30] This is further confirmed by small-angle x-ray scattering data measured for $1.2 \lesssim \zeta \lesssim 1.5$ (Fig. S3 in the supplementary material).

Changes in the intensity are observed under shear depending on the position of the beam along the gap. While the overall intensity is slightly shifted vertically, the shape of the curves only changes in the region around the structure factor peak, 4×10^{-3} Å$^{-1} < Q < 1.4 \times 10^{-2}$ Å^{-1} [Fig. 4(a)]. For smaller and larger Q values, the curves present the same Q dependence, suggesting that shear does not significantly affect the single particle shape, since the decay for $Q > 1.4 \times 10^{-2}$ Å^{-1} has comparable shape. On the contrary, shear flow does affect the overall intensity and S(Q) and, therefore, the local packing fraction and eventually the ordering of the suspension.

To better quantify shear-induced structural changes, the intensities measured under shear, $I(Q)^{sh}$, were divided by a model fit of the I(Q) for the sample at rest, $I(Q)^{rt}_{fit}$ [line in Fig. 4(b), inset], obtaining an excess scattering $I(Q)_{exc} = I(Q)^{sh}/I(Q)^{rt}_{fit}$. A fit was used instead of the experimental data to reduce noise. The model used includes a fuzzy-sphere form factor[41] and a Percus–Yevick hard-sphere structure factor[42] and is reported in Sec. II E. The excess scattering is observed in the Q-range where the effects of S(Q) are present. A separate fit was used for each one of the five positions due to slight fluctuations in the absolute intensity of the quiescent spectrum measured at different positions along the gap.

The values of $I(Q)_{exc}$ depend clearly on the position along the gap, as illustrated in Fig. 4(b) for $\dot{\gamma} = 0.1$ s^{-1} (additional rates are reported in Fig. S5 of the supplementary material). While close to the inner (circles) and outer surfaces (left-side triangles) the excess scattering is close to 1, it increases toward the center (squares and down-side triangles) and reaches a maximum value at the central position (up-side triangles). This behavior indicates that structural variations progressively increase when approaching the center of the gap (up-side triangles), while no significant restructuring is observed compared to the sample at rest in the vicinity of the shearing surfaces (circles and left-side triangles).

The discussed trend can be visualized more clearly by calculating the normalized integral of the excess scattering over the Q range of Fig. 4, $A_{exc} = \int_{Q_1}^{Q_2} I(Q)_{exc}\, dQ / \int_{Q_1}^{Q_2} dQ$, where Q_1 and Q_2 are the smallest and largest Q values, respectively, in Fig. 4. Integration allows us to reduce once more the effect of noise. As shown in Fig. 2(b), a pronounced maximum of A_{exc} is observed at the central position of the gap ($z/z_g \simeq 0.5$), where the velocity profile shows a plug-like response [Fig. 2(a)].

The increase in sample structuring and the linked plug-like response could be associated with particle migration and changes in the local packing fraction. The sample transmission at the different points along the gap is computed to test this hypothesis. As shown in Fig. 2(c), the transmission under shear (T) divided by that at rest (T_0) shows a trend that is inverted compared to A_{exc} with a minimum at $z/z_g \simeq 0.5$, confirming an increase in the local packing fraction in the central region of the gap. While the differences in transmission are rather small, they are not within error bars; moreover, the close connection with variations of A_{exc} supports their significance. The increase in the packing fraction in the central band implies that a related decrease should be observed in some of the other bands: this is indeed confirmed by values of A_{exc} determined at the remaining points, as shown in Fig. S6 of the supplementary material. Additionally, the average value of A_{exc} calculated over the five points along the gap is close to 1 in all cases. These data establish a link between shear banding in the velocity profile and local variations of ϕ_{eff} in the bands. They are also consistent with the increase in the stress observed in the rheological data (Fig. 1).

To investigate how the observed banding depends on the shear rate $\dot{\gamma}$ (Pe_0), we focus on the central region of the velocity profile where the strongest changes in shape and relative velocity are observed, which we associate with structural variations. The diamonds in Fig. 5 show the velocity ratio (v_{lin}/v), i.e., the ratio between the velocity of a linear velocity profile and the measured velocity in the center, as a function of $\dot{\gamma}$. Thus, $v_{lin}/v \neq 1$ indicates the presence of shear banding, with $v_{lin}/v > 1$ corresponding to the presence of slower bands. The fractional part quantifies the amount of deviation from the linear profile. Apart for $\dot{\gamma} = 0.02$ s^{-1}, which might be affected by the stability of the setup in producing the desired displacements at small rates, the remaining values show that the pronounced shear banding observed at $\dot{\gamma} = 0.05$ s^{-1} progressively decreases with increasing shear rate, becoming very weak for $\dot{\gamma} = 1.00$ s^{-1}. Furthermore, the triangles in Fig. 5 represent the values of A^{cb}_{exc} vs $\dot{\gamma}$, i.e., the value of A_{exc} for the mid-position along the gap. Similar to v_{lin}/v, A^{cb}_{exc} monotonically decreases with increasing $\dot{\gamma}$, reaching the smallest value of approximately 1 for $\dot{\gamma} = 0.5$ s^{-1}. Also the value of T/T_0 is found to increase and approach 1 with increasing $\dot{\gamma}$ (Fig. 5, inset).

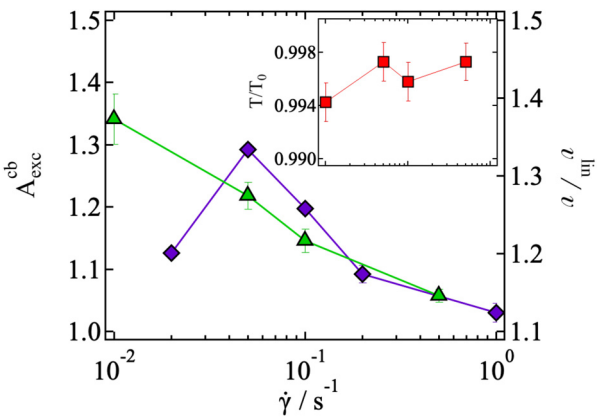

FIG. 5. Integrated excess scattering A_{exc} (triangles, left y-axis) and velocity ratio v^{lin}/v (diamonds, right y-axis) obtained for the central band of the flowing dispersion, as a function of shear rate. Inset: Ratio between the transmissions of the sheared (T) and unsheared (T_0) sample, as a function of shear rate (same x-axis as the main plot).

The consistency in the trends of ν_{lin}/ν and A_{exc}^{cb} further strengthens the proposed link between the laminar or plug-like flow of the central band of the velocity profile, and local variations of ϕ_{eff} and of the structure of the suspension.

The presence of a moderate gradient in the shear rate that is present in the Couette geometry is fundamental to interpret the observed behavior: it has been previously shown that this gradient, although not being strong enough to induce shear localization at the stator,[37,43] can induce particle migration across the gap,[15] leading to an amplification of the shear rate gradient and of the mass flux until the shear-gradient induced mass flux is balanced by the concentration gradient-induced diffusion. This mechanism is called shear concentration coupling.[15] At shear startup, the higher rate close to the moving rotor is expected to induce a faster migration of particles from the inner moving wall toward the center, than from the center toward the outer wall. The compressibility of the microgels might play an important role in facilitating particle rearrangements and migration, compared to hard-sphere like colloids. Migration of particles from the inner wall is expected to induce a faster increase in the packing fraction at the center of the gap, as confirmed by our data. In the vicinity of $\phi_{eff} = 1.3$, the packing fraction of our sample, a transition in the rheological response has been observed in previous measurements,[29] and associated with the limit of compression of the microgel corona and the onset of core compression.[29,44] Variations of the local packing fraction due to particle migration might be responsible for inducing this transition in the central region of the gap and thus for the onset of plug-like flow. Particle migration and associated complex velocity profiles have been also observed in non-Brownian particulate suspensions[43,45,46] and interpreted in terms of the suspension balance model.[47] However, Brownian diffusion plays a key role in our suspensions.

While the origin of the temporal fluctuations in the velocity profile is unclear at the moment, different mechanisms could contribute to establish them: Fluctuations of the local packing fraction in the center of the gap could result from particles amassing close to the wall, and associated vorticity rolling,[48] or by local deswelling due to sudden compression induced by crowding.[49,50] Additional insight into the nature of the observed shear banding and fluctuations will be gathered in the future by measurements of normal stresses and velocity profiles at different heights on the shear cell.

Summarizing these observations, the combination of structural information, velocimetry, and rheology data provides experimental evidence of the shear-concentration coupling mechanism. Particle migration might be favored in microgels by compressibility, that may facilitate rearrangements through particle deswelling and deformation compared to hard-sphere like particles. The observed structural changes are more pronounced than what one could expect on the basis of the measured values of the transmission and, therefore, the increase in the local packing fraction. This suggests that together with the variation of the local packing fraction, also the local ordering of the suspension might increase. The key role of compressibility and of the deformation of individual particles will be systematically investigated in the future by variation of the ϕ_{eff} of the dispersions and the degree of cross-linking of the microgel network, which can be used to finely tune the bulk modulus of the individual particles.[22] However, to have a definitive comparison between the behavior of hard spheres and deformable soft colloids, one must know the real packing fraction occupied by the particle.[51,52] This might be achieved in the future by combining super-resolved microscopy,[20,28] small-angle neutron scattering with contrast variation,[51,53,54] and computer simulations of *in silico* microgels.[55–57]

IV. CONCLUSIONS

In this work, we were able to establish a link between shear band formation, structural changes, and particle migration for dense suspensions of compressible colloids, providing experimental confirmation of the mechanism of shear–concentration coupling.[15,17] Fluctuations in the banding behavior are observed, which could be associated with physical mechanisms inducing variations of the local packing fraction at the center of the gap, like vorticity rolling or local deswelling. These mechanisms need to be investigated in more detail in the future. Additionally, our study opens up the route to investigate the effects of particle compressibility on this mechanism for a variety of dispersions of soft colloids, with important consequences in applications related to the flow and processing of dense suspensions.

SUPPLEMENTARY MATERIAL

See the supplementary material for measurements of hydrodynamic radius by dynamic light scattering; velocity profile for $\dot{\gamma} = 0.5\,s^{-1}$ and long waiting time; SAXS data for different values of the effective volume fraction; SANS measurements at different points along the shear-cell gap and for different shear rates; excess scattering for additional shear rates; excess area for different positions across the gap; and SANS intensities measured for different waiting times after applying shear.

ACKNOWLEDGMENTS

The authors thank Stefan Egelhaaf as a source of continuous inspiration and for illuminating discussions. M.L. and G.B. acknowledge financial support from the European Soft Matter Infrastructure (No. E200100379) for performing velocimetry measurements at FZJ, and partial financial support from Center for Colloid and Surface Science (CSGI). A.S. acknowledges financial support from the Knut and Alice Wallenberg Foundation (Wallenberg Academy Fellows) and from the Deutsche Forschungsgemeinschaft (DFG) within projects A3 and B8 of the SFB 985 – Functional Microgels and Microgel Systems and the Knowledge Foundation (Sweden, Grant Number 20190010). The authors acknowledge the Institut Laue – Langevin for the awarded beamtime (http://doi.ill.fr/10.5291/ILL-DATA.9-10-1752) on the small-angle neutron scattering D22. We acknowledge MAX IV Laboratory for time at the CoSAXS beamline under proposal Nos. 20231840 and 20231866. Research conducted at MAX IV, a Swedish national user facility, is supported by the Swedish Research Council under contract No. 2018-07152, the Swedish Governmental Agency for Innovation Systems under contract No. 2018-04969.

AUTHOR DECLARATIONS

Conflict of Interest

The authors have no conflicts to disclose.

Author Contributions

Gavino Bassu: Data curation (equal); Formal analysis (equal); Investigation (equal); Visualization (equal); Writing – review & editing

(equal). **Judith E. Houston:** Conceptualization (equal); Data curation (equal); Formal analysis (equal); Investigation (equal); Methodology (equal); Resources (equal); Supervision (equal); Validation (equal); Writing – review & editing (equal). **Mayra A. Lara-Peña:** Resources (equal); Writing – review & editing (equal). **Hartmut Kriegs:** Formal analysis (equal); Investigation (equal); Methodology (equal); Resources (equal); Software (equal); Validation (equal). **Minne Paul Lettinga:** Conceptualization (equal); Methodology (equal); Resources (equal); Supervision (equal); Writing – review & editing (equal). **Lionel Porcar:** Conceptualization (equal); Methodology (equal); Resources (equal); Validation (equal); Writing – review & editing (equal). **Andrea Scotti:** Conceptualization (equal); Funding acquisition (equal); Methodology (equal); Project administration (equal); Resources (equal); Supervision (equal); Writing – original draft (equal). **Marco Laurati:** Conceptualization (equal); Funding acquisition (equal); Methodology (equal); Project administration (equal); Resources (equal); Supervision (equal); Writing – original draft (equal).

DATA AVAILABILITY

The data that support the findings of this study are openly available in RADAR4Chem at http://doi.org/10.22000/tdxnuq0xak2mbry9.

REFERENCES

[1]T. Divoux, M. A. Fardin, S. Manneville, and S. Lerouge, "Shear banding of complex fluids," Annu. Rev. Fluid Mech. **48**, 81–103 (2016)..

[2]P. Schall and M. van Hecke, "Shear bands in matter with granularity," Annu. Rev. Fluid Mech. **42**, 67–88 (2010)..

[3]S. M. Fielding, "Shear banding in soft glassy materials," Rep. Prog. Phys. **77**, 102601 (2014).

[4]D. Bonn, M. M. Denn, L. Berthier, T. Divoux, and S. Manneville, "Yield stress materials in soft condensed matter," Rev. Mod. Phys. **89**, 035005 (2017).

[5]T. Divoux, D. Tamarii, C. Barentin, and S. Manneville, "Transient shear banding in a simple yield stress fluid," Phys. Rev. Lett. **104**, 208301 (2010).

[6]P. Chaudhuri and J. Horbach, "Onset of flow in a confined colloidal glass under an imposed shear stress," Phys. Rev. E **88**, 040301 (2013).

[7]R. L. Moorcroft and S. M. Fielding, "Criteria for shear banding in time-dependent flows of complex fluids," Phys. Rev. Lett. **110**, 086001 (2013).

[8]A. R. Hinkle and M. L. Falk, "A small-gap effective-temperature model of transient shear band formation during flow," J. Rheol. **60**, 873–882 (2016). https://pubs.aip.org/sor/jor/article-pdf/60/5/873/16729373/873_1_online.pdf.

[9]L. Bécu, S. Manneville, and A. Colin, "Yielding and flow in adhesive and non-adhesive concentrated emulsions," Phys. Rev. Lett. **96**, 138302 (2006).

[10]M. Cloitre, R. Borrega, and L. Leibler, "Rheological aging and rejuvenation in microgel pastes," Phys. Rev. Lett. **85**, 4819–4822 (2000).

[11]R. Benzi, M. Sbragaglia, M. Bernaschi, S. Succi, and F. Toschi, "Cooperativity flows and shear-bandings: A statistical field theory approach," Soft Matter **12**, 514–530 (2016).

[12]L. Berthier, "Yield stress, heterogeneities and activated processes in soft glassy materials1," J. Phys: Condens. Matter **15**, S933 (2003).

[13]P. Chaudhuri, L. Berthier, and L. Bocquet, "Inhomogeneous shear flows in soft jammed materials with tunable attractive forces," Phys. Rev. E **85**, 021503 (2012).

[14]V. Schmitt, C. M. Marques, and F. m c Lequeux, "Shear-induced phase separation of complex fluids: The role of flow-concentration coupling," Phys. Rev. E **52**, 4009–4015 (1995).

[15]H. Jin, K. Kang, K. H. Ahn, and J. K. G. Dhont, "Flow instability due to coupling of shear-gradients with concentration: Non-uniform flow of (hard-sphere) glasses," Soft Matter **10**, 9470–9485 (2014).

[16]L. Gentile, B. F. B. Silva, S. Lages, K. Mortensen, J. Kohlbrecher, and U. Olsson, "Rheochaos and flow instability phenomena in a nonionic lamellar phase," Soft Matter **9**, 1133–1140 (2013).

[17]R. Besseling, L. Isa, P. Ballesta, G. Petekidis, M. E. Cates, and W. C. K. Poon, "Shear banding and flow-concentration coupling in colloidal glasses," Phys. Rev. Lett. **105**, 268301 (2010).

[18]S. Mandal, M. Gross, D. Raabe, and F. Varnik, "Heterogeneous shear in hard sphere glasses," Phys. Rev. Lett. **108**, 098301 (2012).

[19]A. Scotti, M. F. Schulte, C. G. Lopez, J. J. Crassous, S. Bochenek, and W. Richtering, "How softness matters in soft nanogels and nanogel assemblies," Chem. Rev. **122**, 11675–11700 (2022).

[20]G. M. Conley, C. Zhang, P. Aebischer, J. L. Harden, and F. Scheffold, "Relationship between rheology and structure of interpenetrating, deforming and compressing microgels," Nat. Commun. **10**, 2436 (2019).

[21]G. Chaudhary, A. Ghosh, J. G. Kang, P. V. Braun, R. H. Ewoldt, and K. S. Schweizer, "Linear and nonlinear viscoelasticity of concentrated thermoresponsive microgel suspensions," J. Colloid Interface Sci. **601**, 886–898 (2021).

[22]J. E. Houston, L. Fruhner, A. de la Cotte, J. Rojo González, A. V. Petrunin, U. Gasser, R. Schweins, J. Allgaier, W. Richtering, A. Fernandez-Nieves *et al.*, "Resolving the different bulk moduli within individual soft nanogels using small-angle neutron scattering," Sci. Adv. **8**, eabn6129 (2022).

[23]R. Benzi, T. Divoux, C. Barentin, S. Manneville, M. Sbragaglia, and F. Toschi, "Unified theoretical and experimental view on transient shear banding," Phys. Rev. Lett. **123**, 248001 (2019).

[24]T. Divoux, V. Lapeyre, V. Ravaine, and S. Manneville, "Wall slip across the jamming transition of soft thermoresponsive particles," Phys. Rev. E **92**, 060301 (2015).

[25]A. K. Gurnon, P. D. Godfrin, N. J. Wagner, A. P. R. Eberle, P. Butler, and L. Porcar, "Measuring material microstructure under flow using 1–2 plane flow-small angle neutron scattering," JoVE J. **84**, e51068 (2014).

[26]P. S. Mohanty, S. Nöjd, K. van Gruijthuijsen, J. J. Crassous, M. Obiols-Rabasa, R. Schweins, A. Stradner, and P. Schurtenberger, "Interpenetration of polymeric microgels at ultrahigh densities," Sci. Rep. **7**, 1487 (2017).

[27]A. Scotti, A. R. Denton, M. Brugnoni, J. E. Houston, R. Schweins, I. I. Potemkin, and W. Richtering, "Deswelling of microgels in crowded suspensions depends on cross-link density and architecture," Macromolecules **52**, 3995–4007 (2019).

[28]G. M. Conley, P. Aebischer, S. Nöjd, P. Schurtenberger, and F. Scheffold, "Jamming and overpacking fuzzy microgels: Deformation, interpenetration, and compression," Sci. Adv. **3**, e1700969 (2017).

[29]M. Lara-Peña, A. Licea-Claverie, I. Zapata-González, and M. Laurati, "Colloidal and polymeric contributions to the yielding of dense microgel suspensions," J. Colloid Interface Sci. **587**, 437–445 (2021).

[30]J. Ruiz-Franco, R. Rivas-Barbosa, M. A. Lara-Peña, J. R. Villanueva-Valencia, A. Licea-Claverie, E. Zaccarelli, and M. Laurati, "Concentration and temperature dependent interactions and state diagram of dispersions of copolymer microgels," Soft Matter **19**, 3614–3628 (2023).

[31]A. Serrano-Medina, J. Cornejo-Bravo, and A. Licea-Claveríe, "Synthesis of pH and temperature sensitive, core–shell nano/microgels, by one pot, soap-free emulsion polymerization," J. Colloid Interface Sci. **369**, 82–90 (2012).

[32]R. Rivas-Barbosa, J. Ruiz-Franco, M. A. Lara-Peña, J. Cardellini, A. Licea-Claverie, F. Camerin, E. Zaccarelli, and M. Laurati, "Link between morphology, structure, and interactions of composite microgels," Macromolecules **55**, 1834–1843 (2022).

[33]J. Delgado, H. Kriegs, and R. Castillo, "Flow velocity profiles and shear banding onset in a semidilute wormlike micellar system under Couette flow," J. Phys. Chem. B **113**, 15485–15494 (2009).

[34]C. Pellet and M. Cloitre, "The glass and jamming transitions of soft polyelectrolyte microgel suspensions," Soft Matter **12**, 3710–3720 (2016).

[35]J. Choi and S. A. Rogers, "Optimal conditions for pre-shearing thixotropic or aging soft materials," Rheol. Acta **59**, 921–934 (2020).

[36]B. F. Di Dio, F. Khabaz, R. T. Bonnecaze, and M. Cloitre, "Transient dynamics of soft particle glasses in startup shear flow. Part II: Memory and aging," J. Rheol. **66**, 717–730 (2022). https://pubs.aip.org/sor/jor/article-pdf/66/4/717/16687055/717_1_online.pdf.

[37]G. Ovarlez, S. Rodts, X. Chateau, and P. Coussot, "Phenomenology and physical origin of shear localization and shear banding in complex fluids," Rheol. Acta **48**, 831–844 (2009).

[38]D. Kong, W.-R. Chen, K.-Q. Zeng, L. Porcar, and Z. Wang, "Localized elasticity governs the nonlinear rheology of colloidal supercooled liquids," Phys. Rev. X **12**, 041006 (2022).

[39]M. E. Helgeson, M. D. Reichert, Y. T. Hu, and N. J. Wagner, "Relating shear banding, structure, and phase behavior in wormlike micellar solutions," Soft Matter **5**, 3858–3869 (2009).
[40]C. Lang, L. Porcar, H. Kriegs, and M. P. Lettinga, "A quest for shear banding in ideal and non ideal colloidal rods," J. Phys. D: Appl. Phys. **52**, 074003 (2019).
[41]M. Stieger, W. Richtering, J. S. Pedersen, and P. Lindner, "Small-angle neutron scattering study of structural changes in temperature sensitive microgel colloids," J. Chem. Phys. **120**, 6197–6206 (2004). https://pubs.aip.org/aip/jcp/article-pdf/120/13/6197/10855225/6197_1_online.pdf.
[42]A. Scotti, J. Houston, M. Brugnoni, M. Schmidt, M. Schulte, S. Bochenek, R. Schweins, A. Feoktystov, A. Radulescu, and W. Richtering, "Phase behavior of ultrasoft spheres show stable bcc lattices," Phys. Rev. E **102**, 052602 (2020).
[43]G. Ovarlez, F. Bertrand, and S. Rodts, "Local determination of the constitutive law of a dense suspension of noncolloidal particles through magnetic resonance imaging," J. Rheol. **50**, 259–292 (2006). https://pubs.aip.org/sor/jor/article-pdf/50/3/259/15877300/259_1_online.pdf.
[44]A. Ghosh, G. Chaudhary, J. G. Kang, P. V. Braun, R. H. Ewoldt, and K. S. Schweizer, "Linear and nonlinear rheology and structural relaxation in dense glassy and jammed soft repulsive PNIPAM microgel suspensions," Soft Matter **15**, 1038–1052 (2019).
[45]M. Sarabian, M. Firouznia, B. Metzger, and S. Hormozi, "Fully developed and transient concentration profiles of particulate suspensions sheared in a cylindrical couette cell," J. Fluid Mech. **862**, 659–671 (2019).
[46]G. Ovarlez and E. Guazzelli, "Shear-induced migration of rigid spheres in a Couette flow," J. Rheol. **68**, 913–932 (2024).
[47]P. R. Nott and J. F. Brady, "Pressure-driven flow of suspensions: Simulation and theory," J. Fluid Mech. **275**, 157–199 (1994).
[48]K. Kang, M. P. Lettinga, Z. Dogic, and J. K. G. Dhont, "Vorticity banding in rodlike virus suspensions," Phys. Rev. E **74**, 026307 (2006).
[49]S. Manneville, J. B. Salmon, and A. Colin, "A spatio-temporal study of rheo-oscillations in a sheared lamellar phase using ultrasound," Eur. Phys. J. E **13**, 197–212 (2004).
[50]J.-B. Salmon, S. Manneville, and A. Colin, "Shear banding in a lyotropic lamellar phase. II. Temporal fluctuations," Phys. Rev. E **68**, 051504 (2003).
[51]A. Scotti, "Characterization of the volume fraction of soft deformable microgels by means of small-angle neutron scattering with contrast variation," Soft Matter **17**, 5548–5559 (2021).
[52]M. Pelaez-Fernandez, A. Souslov, L. Lyon, P. M. Goldbart, and A. Fernandez-Nieves, "Impact of single-particle compressibility on the fluid-solid phase transition for ionic microgel suspensions," Phys. Rev. Lett. **114**, 098303 (2015).
[53]S. Nöjd, P. Holmqvist, N. Boon, M. Obiols-Rabasa, P. S. Mohanty, R. Schweins, and P. Schurtenberger, "Deswelling behaviour of ionic microgel particles from low to ultra-high densities," Soft Matter **14**, 4150–4159 (2018).
[54]A. Scotti, U. Gasser, E. S. Herman, M. Pelaez-Fernandez, J. Han, A. Menzel, L. A. Lyon, and A. Fernández-Nieves, "The role of ions in the self-healing behavior of soft particle suspensions," Proc. Natl. Acad. Sci. U. S. A. **113**, 5576–5581 (2016).
[55]N. Gnan, L. Rovigatti, M. Bergman, and E. Zaccarelli, "In silico synthesis of microgel particles," Macromolecules **50**, 8777–8786 (2017).
[56]T. Höfken, C. Strauch, S. Schneider, and A. Scotti, "Changes in the form factor and size distribution of nanogels in crowded environments," Nano Lett. **22**, 2412–2418 (2022).
[57]S. V. Nikolov, A. Fernandez-Nieves, and A. Alexeev, "Behavior and mechanics of dense microgel suspensions," Proc. Natl. Acad. Sci. U. S. A. **117**, 27096–27103 (2020).